

Creep and quakes on the northern transition zone of the San Andreas fault from GPS and InSAR data

I. A. Johanson and R. Bürgmann

Department of Earth and Planetary Science, University of California, Berkeley, California, USA

Received 4 April 2005; revised 28 May 2005; accepted 14 June 2005; published 21 July 2005.

[1] The San Juan Bautista (SJB) segment forms the northern transition zone of the creeping section of the San Andreas fault. It is an area of moderate seismicity; the largest instrumentally-recorded earthquakes have been $M_{5.5}$. However, historic records suggest six $M \geq 6$ earthquakes occurred near the SJB segment between 1840 and 1899. It is also an area that has experienced several slow earthquakes. We perform a joint inversion of GPS and InSAR data to determine the current rate and distribution of interseismic creep. We find two low-slip/locked segments at mid-seismogenic depths that may represent source regions for the 19th century earthquakes. We find that the SJB segment is currently accumulating strain energy at the rate of one $M_{6.3-6.7}$ earthquake per century. At this rate, the 1840–1899 sequence released 135–510 years of accumulated moment deficit. **Citation:** Johanson, I. A., and R. Bürgmann (2005), Creep and quakes on the northern transition zone of the San Andreas fault from GPS and InSAR data, *Geophys. Res. Lett.*, *32*, L14306, doi:10.1029/2005GL023150.

1. Introduction

[2] Surface creep on the San Juan Bautista (SJB) segment has been studied since the 1960's with both creepmeters and alignment array surveys (see *Bokelmann and Kovach* [2003] and *Galehouse and Lienkaemper* [2003] for summaries). These creepmeter records include observations of episodic creep, which take place over hours to days and involve slip in the upper 500 m of the fault [*Gladwin et al.*, 1994]. In 1992, a slow earthquake was detected on the SJB segment by creepmeters and strainmeters. This event occurred in the same section of the fault as the episodic creep, but involved transient slip down to a depth of 4–8 km [*Linde et al.*, 1996]. Further slow earthquakes have occurred in 1996, 1998, 2003 and 2004, with equivalent magnitudes of $M_w \sim 5$, and on time scales of weeks [*Gwyther et al.*, 2000; *Gladwin*, 2004]. Surface creep rates significantly accelerated along the SJB segment, in response to the 1989 Loma Prieta earthquake, and have not returned to pre-earthquake levels [*Behr et al.*, 1997; *Bokelmann and Kovach*, 2003].

[3] The largest recent earthquake on the SJB segment was a $M_w 5.1$ event which immediately preceded the 1998 slow earthquake [*Gwyther et al.*, 2000; *Uhrhammer et al.*, 1999]. However, historic records indicate that the SJB segment produced a series of six $M \geq 6$ earthquakes between 1840 and 1899 [*Toppozada et al.*, 2002]. Since then, *Toppozada et al.* [2002] report only two $M_{5.8}$ earthquakes in 1910 and 1916 in the same area. Given the history of slip transients in the SJB area, does the seismic quiescence of the 20th

century, relative to the 19th century, indicate that the amount of creep has increased, possibly in response to increased stress on the SJB segment from the 1906 San Francisco earthquake? In this study, we use a decade of GPS and SAR data to determine the subsurface distribution and rate of creep. The slip model illuminates the relationship between subsurface creep, slow earthquakes, and earthquakes. We estimate a slip budget for the SJB segment to determine if current creep conditions would allow a similar rate of large earthquake production as seen in the 19th century.

2. Data

2.1. GPS Data

[4] We completed campaign GPS surveys in 2001, 2002, and 2003 of up to 50 benchmarks throughout the southern Bay Area. These sites had previous observations from as far back as 1994. The data is processed in GAMIT together with BARD and IGS stations to produce daily unconstrained solutions. The daily solutions are combined with data from throughout the San Francisco Bay Area in the BÄVÜ dataset [*d'Alessio et al.*, 2005] and stabilized in a North American reference frame using GLOBK. More detail on the data and data processing is available from *d'Alessio et al.* [2005]. The GPS velocities (and InSAR range-change rate samples) used in this study are available in the auxiliary materials.¹

2.2. InSAR Data

2.2.1. Interferogram Processing

[5] We complement the high-precision GPS velocities with high-spatial-resolution InSAR range-change rates (change in line-of-sight distance between the satellite and the ground). A set of 10 ERS1 & ERS2 scenes were processed using the ROI_PAC software developed at JPL. The contribution of topography to the interferogram phase was removed using a USGS 30 m DEM. ROI_PAC re-estimates satellite orbit parameters by fitting and removing a low-order polynomial from the interferogram phase data. We preserve the phase gradient due to regional deformation by removing a GPS derived model of interseismic deformation before orbit parameter re-estimation and replacing it after phase unwrapping. Phase unwrapping was performed using SNAPHU [*Chen and Zebker*, 2001].

2.2.2. Stacking and Sampling

[6] The challenge in applying InSAR data to study interseismic deformation is that the tectonic signal is generally very small, producing less than one phase cycle of range-change per year, and is easily obscured by atmospheric delay

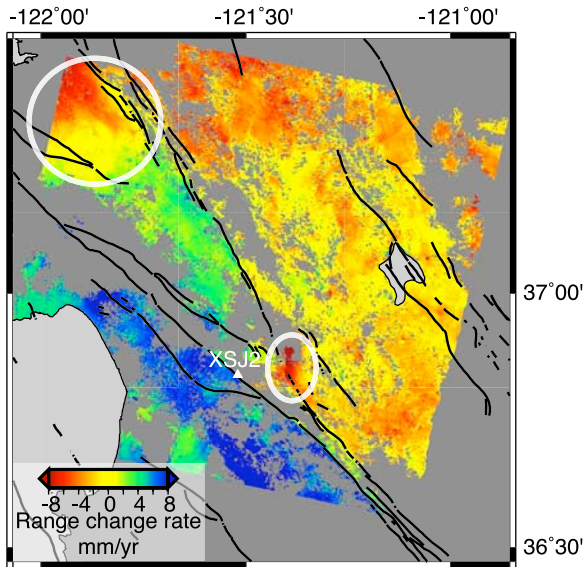


Figure 1. InSAR stack from data spanning 5.75 years, scaled to yearly rate. White circles outline the Hollister and Santa Clara Valley Basins where groundwater recharge results in non-tectonic uplift. These and other areas located on Quaternary sediment were removed before the model inversion (see section 2.2.3). White triangle is the location of creepmeter XSJ2, used as the origin for Figure 3.

errors. Furthermore, in the San Juan Bautista area, interferometric pairs spanning more than a year suffer from severe temporal decorrelation, leading to poor spatial coherence. We address both of these problems by stacking together short time-span pairs. We choose our input interferograms such that the ending scene in one pair is the beginning scene in the next (Table S1). With this selection method, atmospheric errors from repeated dates cancel each other and the stack is equivalent to a single 5.75 year interferogram. The nine interferograms are georeferenced, added together and scaled by the total time span to produce a map of yearly range-change rates (Figure 1). Areas which could not be unwrapped in any single interferogram were not included in the final stack.

[7] The stack is subsampled to reduce the number of observations to a computationally tenable number and to account for correlations between samples introduced by filtering, resampling to the DEM spacing and by any remaining atmospheric errors. We sample on a grid with 500 meter spacing within a 75×25 km box around the SJB segment and on a 2 km spaced grid outside this box. The denser near-fault spacing increases our resolution on the SJB segment, while the sparser far-field spacing provides information on the regional fault system. Because the actual uncertainties in the InSAR data are not well known, we estimate them from the variance of the 25 pixel values averaged within each sample.

2.2.3. Non-Tectonic, Vertical Motion

[8] The Hollister/San Juan valley basin (Figure 1) demonstrates vertical motions associated with groundwater movement. We use only one satellite configuration (descending orbit) and so cannot uniquely isolate non-tectonic vertical motion in the InSAR data. Groundwater-induced vertical motion is the result of expansion and compaction of uncon-

solidated sediment; therefore we remove all InSAR data points which occur on Quaternary sediments (as identified by Jennings [1977]) from our model inversions. This conservative method removes both the data influenced by non-tectonic motion in the Hollister/San Juan valley and any other as yet unidentified area susceptible to groundwater-induced vertical motion.

3. Model Formulation

[9] We formulate our inversion using the equations of Okada [1985] for deformation at the surface of a homogeneous, isotropic, elastic half-space due to slip on embedded dislocations. Deep dislocations (below locking depth to 3000 km) simulate strain accumulation on the regional fault system, including the San Andreas, Calaveras, Paicines, Sargent and Hayward faults (see auxiliary materials, Figure S3). Shallow dislocations (above locking depth) are included on the Calaveras fault and the SJB and Santa Cruz segments of the San Andreas fault. We base our choice of locking depth on estimates by *d'Alessio et al.* [2005], which are based on the depth distribution of seismicity and surface heat flow data. The shallow San Andreas fault along the SJB segment and a portion of the Santa Cruz segment to the north is discretized into 174 2.5×1.5 km elements. The strike of each element in the top two rows closely matches the mapped surface trace of the San Andreas fault, while the deeper elements match only larger changes in strike. We set up our inversion using the method of *Price and Bürgmann* [2002], such that we solve the following equation for optimal slip rate values that minimize the weighted residual sum of squares (WRSS) while seeking a smooth slip rate distribution on the discretized SJB segment.

$$\begin{bmatrix} \mathbf{W}_g \mathbf{G}_g \\ \alpha \mathbf{W}_s \mathbf{G}_s \\ \beta \nabla^2 \end{bmatrix}^{-1} \begin{bmatrix} \mathbf{W}_g \vec{\mathbf{d}}_g \\ \alpha \mathbf{W}_s \vec{\mathbf{d}}_s \\ \mathbf{0} \end{bmatrix} = \begin{bmatrix} \vec{\mathbf{s}} \\ \vec{\mathbf{t}} \end{bmatrix}$$

$\vec{\mathbf{d}}_g$ is the vector of GPS velocities in the east and north directions and $\vec{\mathbf{d}}_s$ contains the InSAR range-change rate samples. \mathbf{G}_g and \mathbf{G}_s are the design matrices of Green's functions, which relate unit slip on each dislocation to displacements or range-change at each observation point. \mathbf{G}_s also contains elements to solve for an offset and linear slope ($\vec{\mathbf{t}}$) to further compensate for residual errors in the satellite orbit parameters that would result in a phase gradient across the InSAR stack. The data and design matrices are internally weighted by the inverse covariance matrix (χ^{-1}) such that

$$\mathbf{W}_{g/s}^T \mathbf{W}_{g/s} = \chi_{g/s}^{-1}$$

α weights the entire InSAR dataset relative to the GPS data. We choose $\alpha = 1.85$, which gives similar WRSS for each data set (518 and 556 for the GPS and InSAR data respectively). We apply a positivity constraint to all dislocations using a bounded variable least squares algorithm [Stark and Parker, 1995] and impose a slip rate of 35 mm/yr on the deep creeping section [Ben-Zion et al., 1993] to compensate for sparse data coverage in that area. β is the weight given to the Laplacian smoothing operator (∇^2), which was applied to only the discretized elements in the

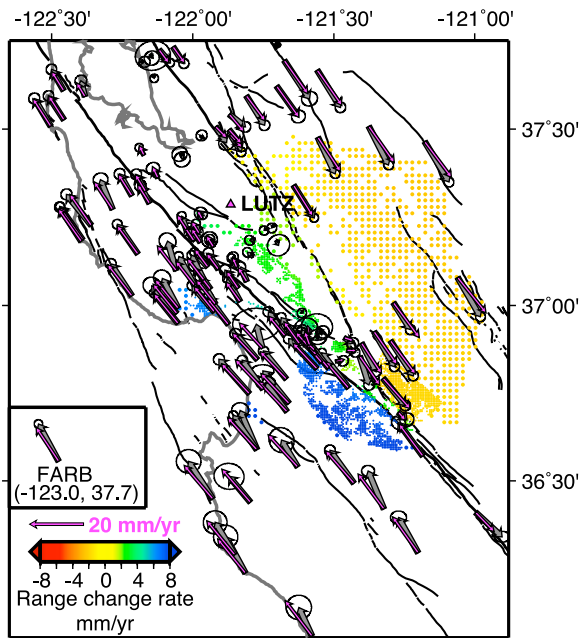


Figure 2. Observed GPS velocities (grey arrows) with 95% confidence ellipses, and model fits to InSAR range change rates and GPS velocities (thinner purple arrows). GPS velocities are relative to station LUTZ (purple triangle).

SJB area. β was chosen by examining a trade-off curve of roughness vs. WRSS for joint inversions (Figure S1). Model fits are shown in Figure 2 and Figure S2.

4. Results and Discussion

4.1. San Juan Bautista Creep Distribution

4.1.1. Relationship to Seismicity

[10] Our model resolves 19.9 ± 1.4 mm/yr of creep on the shallow creeping section, decreasing gradually to the north

along the discretized SJB segments. 12 km north of XSJ2 (Figure 3), the majority of the fault surface is locked, including the source area of the 1990 Chittenden earthquake sequence. Two low-creep/locked asperities occur at mid-seismogenic depths (asperities A and B in Figure 3), which may be source regions for moderate to large earthquakes. However, there is significant uncertainty in the locations of the historic events, such that we cannot assign them to a particular asperity. The decrease in subsurface creep north of the creeping section into asperity B corresponds well with an area of little microseismicity. Similarly, the bottom edge of asperity B also matches well with the depth where microseismic activity occurs in this area. This supports the idea that on creeping faults there is an inverse relationship between microseismicity and locked, earthquake-producing asperities.

4.1.2. Relationship to Slow Earthquakes

[11] Two slow earthquakes occurred on the SJB segment during the time spanned by our GPS and InSAR data. The slip from these slow earthquakes is averaged into our yearly slip rates. Nonetheless, the contributions from these events are not enough to account for all of the creep in the model elements in which they occur. The 1998 slow earthquake slipped 20 mm at the edge of asperity B, contributing 3.5 mm/yr to the inferred creep rate (Figure 3). The 1996 slow earthquake occurred on a creeping portion of the fault, between asperity A and the northern terminus. The locations of the slow earthquakes are consistent with the view that slow earthquakes occur in creeping areas of the fault rather than slipping otherwise locked sections.

4.2. Moment Deficit on the San Juan Bautista Segment

[12] We seek to determine whether a sequence of earthquakes, similar to that seen in the 19th century, could occur on the SJB segment under its current creep conditions. We consider six earthquakes from the catalog of *Topozada et al.* [2002] that locate within 5 km of the SJB segment surface trace. We calculate moment deficit rates for the $i =$

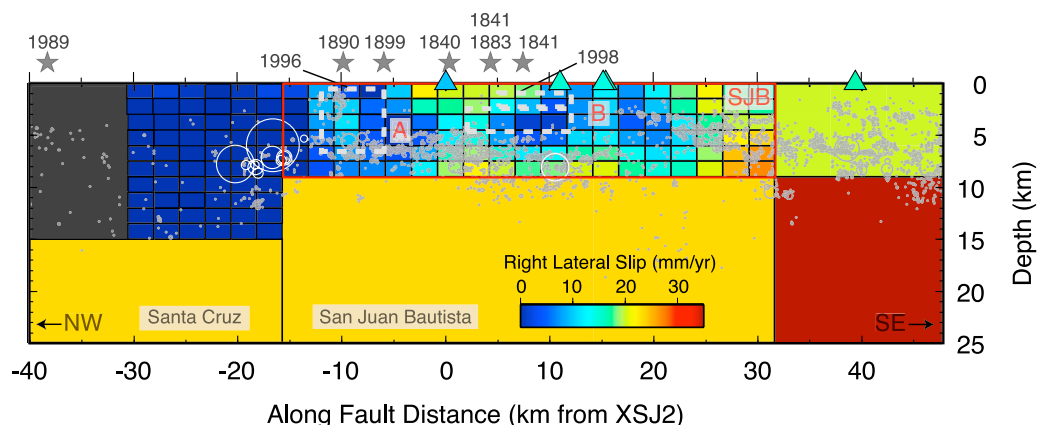


Figure 3. Results of model inversion for the SJB segment. Cross-section is plotted looking north-eastward. Surface creep rates from line fits to creepmeter data from 1994–2001 are shown for comparison (colored triangles). The rupture areas for slow earthquakes in 1996 and 1998 are outlined in dashed grey lines [Gwyther *et al.*, 2000]. Red outline is the shallow SJB segment used to calculate moment deficit. Letters indicate asperities A & B. Grey circles are double-difference relocated earthquakes [Waldhauser and Ellsworth, 1999], white circles 20 km north of XSJ2 are the 1990 Chittenden swarm, the white circle 10 km south of XSJ2 is the 1998 M_w 5.1 San Juan Bautista earthquake. Grey stars are the projected locations of $M \geq 6$ earthquakes within 5 km of the San Andreas fault surface trace from *Topozada et al.* [2002]. Black area signifies that no slip rate was estimated for that fault region.

114 model elements in the shallow SJB segment (large red box in Figure 3) using

$$\dot{M}_{o(\text{deficit})} = \sum_i \mu A_i (\dot{s}_{it} - \dot{s}_i)$$

The long-term slip rate (\dot{s}_{it}) on the deep SJB and Santa Cruz segments is determined to be 23.3 mm/yr in the joint inversion and 16.8 mm/yr in a GPS-only inversion. Both of these rates are close to the expected range for the peninsular San Andreas fault [Hall *et al.*, 1999], so we perform the moment deficit calculations twice, using each of these rates. We also perform the calculations for two values of rigidity (μ), 15 and 25 GPa, reflecting the seismic velocity contrast across the San Andreas fault in this area [Dorbath *et al.*, 1996]. We report the lowest and highest deficit rates from this set of input parameters.

[13] The shallow SJB segment creeps at an average rate of 11.7 mm/yr, which leaves 5.1–11.5 mm/yr of slip deficit and a moment deficit rate of 3.3×10^{23} – 1.2×10^{24} dyne · cm/yr. At this rate the region could produce one M_w 6.3–6.7 earthquake every century and it would take 135–510 years to accumulate the moment released in the 19th century sequence. That the 19th century sequence released hundreds of years worth of accumulated slip deficit is consistent with the relative quiescence observed in the 20th century, and does not indicate that creep has become more widespread. Our data samples post-Loma Prieta creep rates; pre-Loma Prieta surface creep rates were as much as 30% lower [Bokelmann and Kovach, 2003]. At 30% lower creep rates the 19th century earthquake sequence would still represent 105–300 years of moment accumulation.

[14] It is interesting that the historic earthquakes occurred as a clustered sequence rather than a relatively regular series, such as is observed on the Parkfield segment. The Parkfield segment is similarly located at the southern end of the creeping section and is partially locked along a ~25 km-long transition zone [Murray and Segall, 2002]. Based on our results, the ~50 km-long SJB segment could produce a Parkfield-like event (M_w 6.0) every 10–38 years, a similar repeat time to that found by Murray and Segall [2002] of 7–21 years for the Parkfield segment. Unlike Parkfield, the SJB segment is divided into two asperities surrounded by creep. Toppozada *et al.* [2002] note that the historic events all occurred close in time to either the 1906 event or the 1838 M_w 7.4 earthquake on the San Andreas fault (both with southern terminations near San Juan Bautista) suggesting that this segment is sensitive to changes in input stress. Variability in the creep rates on the fault area surrounding the isolated asperities, in response to large earthquakes (such as observed following the Loma Prieta earthquake) could be responsible for loading the asperities in a non-uniform manner [Ben-Zion *et al.*, 1993].

5. Conclusions

[15] While there is significant uncertainty in the location of historic earthquakes near San Juan Bautista, the number of large 19th century events attributed to this segment stands in contrast to the instrumentally observed seismicity.

Our study shows that given the current distribution of creep, the SJB segment is accumulating a moment deficit at the rate of one M_w 6.3–6.7 earthquake per century. The relative quiescence of the 20th century does not appear to be associated with enhanced aseismic moment release. Our model shows two separate low-creep/locked asperities, which could rupture independently of each other. The loading rate is similar to that seen on the Parkfield segment, but the SJB segment does not experience regularly occurring M_w 6 earthquakes. Instead the segment appears to release centuries worth of strain accumulation in clusters that span decades and in response to stress changes from larger events.

[16] **Acknowledgments.** This work was supported by funding from USGS NEHRP grant 04-HQGR-0119 and NSF grant EAR-0337308. SAR data was made available by the WINSAR consortium. We thank Suzanne N. Lyons and an anonymous reviewer for their helpful comments. BSL publication no. 05-11.

References

- Behr, J., R. Bilham, P. Bodin, K. S. Breckenridge, and A. G. Sylvester (1997), Increased surface creep rates on the San Andreas fault southeast of the Loma Prieta main shock, *U.S. Geol. Surv. Prof. Pap.*, 1550-D, D179–D192.
- Ben-Zion, Y., J. R. Rice, and R. Dmowska (1993), Interaction of the San Andreas fault creeping segment with adjacent great rupture zones and earthquake recurrence at Parkfield, *J. Geophys. Res.*, 98(B2), 2135–2144.
- Bokelmann, G. H. R., and R. L. Kovach (2003), Long-term creep-rate changes and their causes, *Geophys. Res. Lett.*, 30(8), 1445, doi:10.1029/2003GL017012.
- Chen, C. W., and H. A. Zebker (2001), Two-dimensional phase unwrapping with use of statistical models for cost functions in nonlinear optimization, *J. Opt. Soc. Am. A Opt. Image Sci.*, 18(2), 338–351.
- d'Alessio, M., I. A. Johanson, R. Bürgmann, D. A. Schmidt, and M. H. Murray (2005), Slicing up the San Francisco Bay Area: Block kinematics and fault slip rates from GPS-derived surface velocities, *J. Geophys. Res.*, 110, B06403, doi:10.1029/2004JB003496.
- Dorbath, C., D. Oppenheimer, F. Amelung, and G. King (1996), Seismic tomography and deformation modeling of the junction of the San Andreas and Calaveras faults, *J. Geophys. Res.*, 101(B12), 27,917–27,941.
- Galehouse, J. S., and J. J. Lienkaemper (2003), Inferences drawn from two decades of alignment array measurements of creep on faults in the San Francisco Bay region, *Bull. Seismol. Soc. Am.*, 93(6), 2415–2433.
- Gladwin, M. T. (2004), Maintenance, data archive and analysis of existing low-frequency GTSM installations in California, National Earthquake Hazards Reduction Program annual project summary, U.S. Geol. Surv., Reston, Va.
- Gladwin, M. T., R. L. Gwyther, R. H. G. Hart, and K. S. Breckenridge (1994), Measurements of the strain field associated with episodic creep events on the San Andreas fault at San Juan Bautista, California, *J. Geophys. Res.*, 99(B3), 4559–4565.
- Gwyther, R. L., C. H. Thurber, M. T. Gladwin, and M. Mee (2000), Seismic and aseismic observations of the 12th August 1998 San Juan Bautista, California M_w 5.3 earthquake, paper presented at 3rd San Andreas Fault Conference, Stanford Univ., Stanford, Calif.
- Hall, N. T., R. H. Wright, and K. B. Clahan (1999), Paleoseismic studies of the San Francisco Peninsula segment of the San Andreas fault zone near Woodside, California, *J. Geophys. Res.*, 104(B10), 23,215–23,236.
- Jennings, C. (1977), Geologic map of California, Geologic data map series, Calif. Dep. of Conserv., Div. of Mines and Geol., Sacramento.
- Linde, A. T., M. T. Gladwin, M. J. S. Johnston, R. L. Gwyther, and R. G. Bilham (1996), A slow earthquake sequence on the San Andreas fault, *Nature*, 383(6595), 65–68.
- Murray, J., and P. Segall (2002), Testing time-predictable earthquake recurrence by direct measurement of strain accumulation and release, *Nature*, 419(6904), 287–291.
- Okada, Y. (1985), Surface deformation due to shear and tensile faults in a half-space, *Bull. Seismol. Soc. Am.*, 75(4), 1135–1154.
- Price, E. J., and R. Bürgmann (2002), Interactions between the Landers and Hector Mine, California, earthquakes from space geodesy, boundary element modeling, and time-dependent friction, *Bull. Seismol. Soc. Am.*, 92(4), 1450–1469.

- Stark, P. B., and R. L. Parker (1995), Bounded-variable least-squares—An algorithm and applications, *Comput. Stat.*, *10*(2), 129–141.
- Topozada, T. R., D. M. Branum, M. S. Reichle, and C. L. Hallstrom (2002), San Andreas fault zone, California: $M \geq 5.5$ earthquake history, *Bull. Seismol. Soc. Am.*, *92*(7), 2555–2601.
- Uhrhammer, R., L. S. Gee, M. H. Murray, D. Dreger, and B. Romanowicz (1999), The Mw 5.1 San Juan Bautista, California earthquake of 12 August 1998, *Seismol. Res. Lett.*, *70*(1), 10–18.
- Waldhauser, F., and W. L. Ellsworth (1999), A double difference earthquake location algorithm; method and application to the San Andreas and Hayward faults, California, *Eos Trans. AGU*, *80*(46), 705.
-
- R. Bürgmann and I. A. Johanson, Department of Earth and Planetary Science, University of California, Berkeley, 307 McCone Hall, Berkeley, CA 94720, USA. (ingrid@seismo.berkeley.edu)